Available online at www.sciencedirect.com
SCIENCE DIRECT®
Thermochimica Acta 411 (2004) 21–26
thermochimica acta
www.elsevier.com/locate/tca

The phase diagram of KNO_3–$KClO_3$

Xuejun Zhang [a,*], Jun Tian [a], Kangcheng Xu [b], Yici Gao [b]

[a] State Key Laboratory of Solid Lubrication, Lanzhou Institute of Chemical Physics, Lanzhou 730000, China
[b] College of Chemistry and Chemical Engineering, Lanzhou University, Lanzhou 730000, China

Received 3 December 2002; received in revised form 30 June 2003; accepted 21 July 2003

Abstract

The binary phase diagram of KNO_3–$KClO_3$ is studied by means of differential scanning calorimetry (DSC) and high-temperature X-ray diffraction. The limited solid solutions, $K(NO_3)_{1-x}(ClO_3)_x$ ($0 < x < 0.20$) and $K(NO_3)_{1-x}(ClO_3)_x$ ($0.90 < x < 1.0$), were formed in the KNO_3-based solid solutions and $KClO_3$-based solid solutions phase, respectively. For KNO_3-based solid solutions, KNO_3 ferroelectric phase can be stable from 423 to 223 K as a result of substituting of NO_3 by ClO_3-radicals. The temperatures for solidus and liquidus have been determined based on limited solid solutions. Two models, Henrian solution and regular solution theory for KNO_3-based (α) phase and $KClO_3$-based (β) phase, respectively, are employed to reproduce solidus and liquidus of the phase diagram. The results are in good agreement with the DSC data. The thermodynamic properties for α and β solid solutions have been derived from an optimization procedure using the experimental data. The calculated phase diagram and optimized thermodynamic parameters are thermodynamically self-consistent.

Keywords: Phase diagram; Limited solid solutions; DSC; HT-XRD; KNO_3–$KClO_3$ system; Ferroelectricity

1. Introduction

Phase diagrams and thermodynamic properties of molten salt systems are necessary information for many electrochemical applications. The phase diagrams that are related to KNO_3 continue to be the subject of intense research activity because of the possibility to use this material in its ferroelectric phase for fabrication of nonvolatile random access memory devices by solid solutions [1]. Under atmospheric pressure, KNO_3 exhibits an interesting phase sequence depending upon the dynamic thermal process. It has an aragonite structure (phase II) at room temperature. When heated, it undergoes a transformation around 130 °C to a rhombohedral structure (phase I). On cooling from some high temperature, e.g., 170 °C, KNO_3 in phase I passes through ferroelectric phase (phase III) before reverting to phase II [2]. The stability and the temperature range existence of the ferroelectric phase (phase III) of KNO_3 should be important for its use. The methods of stabilizing ferroelectric phase (phase III) of KNO_3 are solid solutions, thin film and doping [3]. Most useful ferroelectrics are solid solutions rather than pure-order compounds. The phase transition of KNO_3 is accompanied with reconstruction of atomic configuration of NO_3-radicals. Substitutions of NO_3 by other radicals are expected to influence the transitions of KNO_3. Ferroelectricity of solid solutions, KNO_3–KNO_2 [4], and KNO_3–KI [5], have been studied, and it was found that the temperature range of phase III extended for most cases, especially by lowering of the II–III transition temperature (abbreviated to $T_{II–III}$). Recently, some researchers have noted that there are solid solutions formed in KNO_3-rich regions. Takeuchi [6] got the solid solutions $K(NO_3)_{1-x}(ClO_3)_x$ ($0 < x < 0.07$). A year later, the limit of solid solutions $K(NO_3)_{1-x}(ClO_3)_x$ was extended to $0 < x < 0.20$ [7]. In the solid solutions $K(NO_3)_{1-x}(ClO_3)_x$ ($0 < x < 0.20$), a ferroelectric phase isostructural with phase III of potassium nitrate was found to exist over a wide temperature range. However, the system of KNO_3–$KClO_3$ is usually regarded as a simple eutectic one [8]. No further thermal measurements have been attempted to explore the real range of the solid solutions.

In this work, we determined the phase diagram of KNO_3–$KClO_3$ by differential scanning calorimetry (DSC) and high-temperature X-ray diffraction. Also, this phase diagram was calculated. Experimental results are compared with the predictions of the Henrian solutions and regular solution theory models based on limited solid solutions.

* Corresponding author. Fax: +86-931-8277088.
E-mail address: zhaxj@yahoo.com (X. Zhang).

0040-6031/$ – see front matter © 2003 Elsevier B.V. All rights reserved.
doi:10.1016/j.tca.2003.07.006

2. Experimental

The thermal analyses were carried out on a Perkin-Elmer DSC-7 differential scanning calorimeter. The calibration of the instrument was made by high purity indium and zinc as standard samples.

Reagent grade potassium nitrate and potassium chlorate were recrystallized from redistilled water and dried by heating at approximately 378 K for 3 days. The dried chemicals were weighed at 5% mole intervals, mixed well and transferred to quartz crucibles. The mixtures were thermally cycled, repeated from 378 K for 1 day, through 560 K for 8 h, and at about 20 K above their melting points for at least 8 h to achieve well-mixed and homogenous compositions for the mixtures. Then the quenched samples were ground into a fine powder and stored in desiccator.

At least three successive runs were carried out for each sample. Generally, the results of the third run were in good agreement with those of the second run (indicating equilibrium conditions) and only the data of third run are reported. The liquidus data was established by cooling the melts after they were held at about 20 K above their melting points for at least 5 min. DSC energy scales (0.5–5 mcal s^{-1}), and the N_2 sweep rate through the DSC assembly was ~20 cm^3 min^{-1}, the samples (5–20 mg) were placed in open aluminum pans. We made many DSC profiles of the salt mixtures using different heating and cooling rates (1.5–20 K min^{-1}) to find consistent results for the liquidus and solidus.

High-temperature powder XRD pattern of samples, $x_{KClO_3} = 0.05$, 0.20 was recorded in static air in the range of $22^\circ < 2\theta < 40^\circ$ with a scan rate of 1° min^{-1} and the heating/cooling rate of 5 K min^{-1} using Cu Kα radiation on a Philips X-ray diffractometer Model X'Pert MPD. The high temperature X-ray powder diffraction studies were carried out using an MRC Model X-86-N3 high-temperature diffractometer attachment. A small amount of finely ground sample was mounted on a Pt–40% Rh stage as heating element. A Pt/Pt–13% Rh thermocouple, spot welded to the bottom of the stage, was used for the temperature measurement. The temperature was controlled with an MRC Model proportional temperature controller.

3. Thermodynamic relationships

For equilibrium between a solid and a liquid phase in a binary system with components A and B, the Gibbs energy of fusion of A may be expressed as

$$-\Delta_{fus}G_A = \frac{RT\ln x_A(l)}{x_A(s)} + G_A^E(l) - G_A^E(s) \quad (1)$$

where $x_A(l)$ and $x_A(s)$ are the mole fractions of A on the liquidus and solidus at temperature T, respectively, and R is the gas constant. $G_A^E(l)$ and $G_A^E(s)$ are the partial excess Gibbs energies of A in the liquid and solid. In this system the excess entropy $S^E(l)$ and $S^E(s)$ were set equal to zero. So $G^E = H^E$. The partial properties can be obtained from the integral property from the following equation:

$$G_i^E = H_i^E = H^E + (1 - x_i)\frac{dH^E}{dx_i} \quad (2)$$

where i = A or B.

H^E may be expanded as polynomials in the mole fractions as follows [9]:

$$H^E = x_A x_B(h_0 + h_1 x_B + \cdots + h_i x_B^i) \quad (3)$$

where the h_i are empirical coefficients.

4. Results and discussion

Typical DSC curves in Fig. 1, obtained in a Perkin-Elmer DSC-7 with sample masses of 20 mg and scanning rates of 5 K min^{-1}, show the phase transition behavior of quenched $K(NO_3)_{1-x}(ClO_3)_x$ ($x = 0.1$) solid solution. That behavior is similar to the behavior of pure powder KNO_3 at atmospheric pressure. But the phase transition temperatures of phase II to phase I and phase I to phase III are all higher in $K(NO_3)_{1-x}(ClO_3)_x$ solid solutions than in pure KNO_3. The phase III to phase II transition in $K(NO_3)_{1-x}(ClO_3)_x$ solid solutions had not been found by DSC.

The data for solidus and the data for liquidus are listed in Table 1 and graphically displayed in Fig. 2. The solidus is nearly horizontal in the composition from 20 to 90 mol% $KClO_3$. The eutectic temperature is 556 K at $x_B = 0.30$ and the limits of solid solubility at the eutectic temperature are $x_B = 0.20$ and 0.90, respectively.

Figs. 3 and 4 show qualitative powder diffractograms corresponding to one cycle of heating and cooling of the samples, $x_{KClO_3} = 0.05$ and 0.20 for the mixture of KNO_3 and $KClO_3$, respectively. The absence of the $KClO_3$ solid phase different from the solid solution phase is evident. Moreover, powder diffractograms demonstrate the existence of a true solid solution, i.e. not a simple mixture of endmembers, KNO_3 and $KClO_3$. The clear and continuous shift towards

Table 1
DSC data for the KNO_3–$KClO_3$ system

Mole fraction of $KClO_3$	Solidus temperature, T_S (K)	Liquidus temperature, T_L (K)
0		608
0.05		591.8
0.1		582.5
0.2	557	564.8
0.3	558	558
0.4	557.3	566
0.5	556	580
0.6	556.1	589
0.7	558.1	594
0.8	557	610
0.9		619
0.95		623
1		641

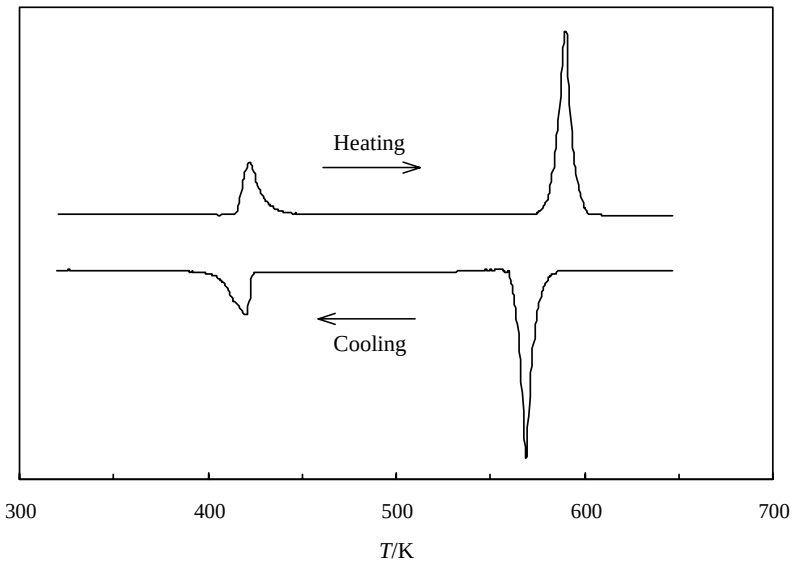

Fig. 1. Typical DSC profiles of $K(NO_3)_{1-x}$ ($x = 0.1$) solid solution during third heating and cooling runs.

lower 2θ angles when the chlorate anion mole fraction increases is the result of the unit cell enlargement promoted by substitution of nitrate anion by chlorate anion. The presence of a small feature close to 25.8°, in the diffractogram corresponding to the 20% sample, could be explained as an effect of the other solid solution, $KClO_3$-based solid solutions. The presence of an impurity can be ruled out because no other extra band appears in none of the diffraction patterns. The half-width of the 20% sample diffraction peaks is larger than one of the 5% sample, which is the result of the anionic positional disorder by chlorate anionic substitution.

During heating of the samples, $x_{KClO_3} = 0.05$ and 0.20 (Figs. 3a and 4a), the KNO_3 (II) to KNO_3 (I) phase transitions occur at 423 K, the ferroelectric phase KNO_3 (III) was not detected. These phase transitions resemble ones of pure KNO_3. But during cooling, the solid solution phase transitions were different from pure KNO_3. The KNO_3 (I) to KNO_3 (III) phase transitions occur at 423 K and the phase KNO_3 (III) was stabilized down to 223 K by the solid solutions $K(NO_3)_{1-x}(ClO_3)_x$ (Figs. 3b and 4b), which was at room temperature reported previously [6,7]. Since the ionic radius of ClO_3^- is larger than that of NO_3^-, the structure of the solid solutions $K(NO_3)_{1-x}(ClO_3)_x$ ($0 < x < 0.20$) constrained internal stress, which may be the reason for the stabilization of the KNO_3 ferroelectric phase below room temperature.

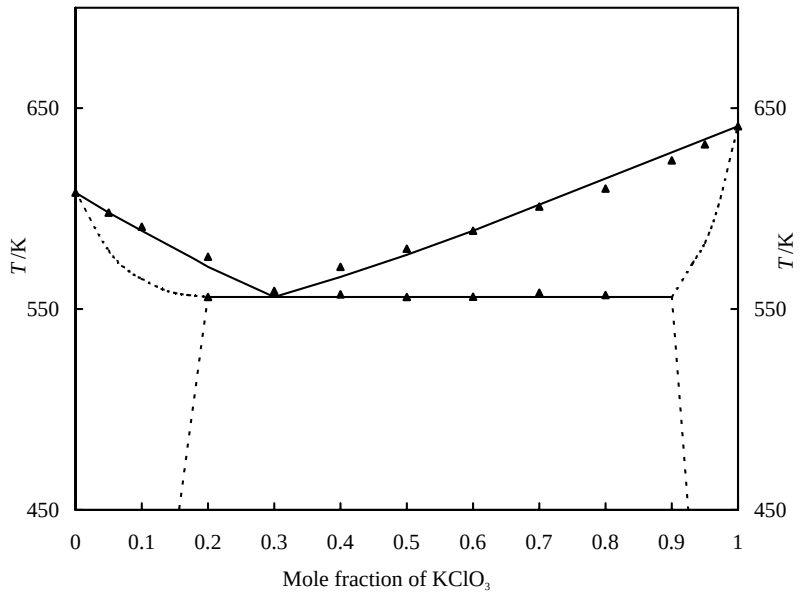

Fig. 2. The phase diagram for the KNO_3–$KClO_3$ system during heating.

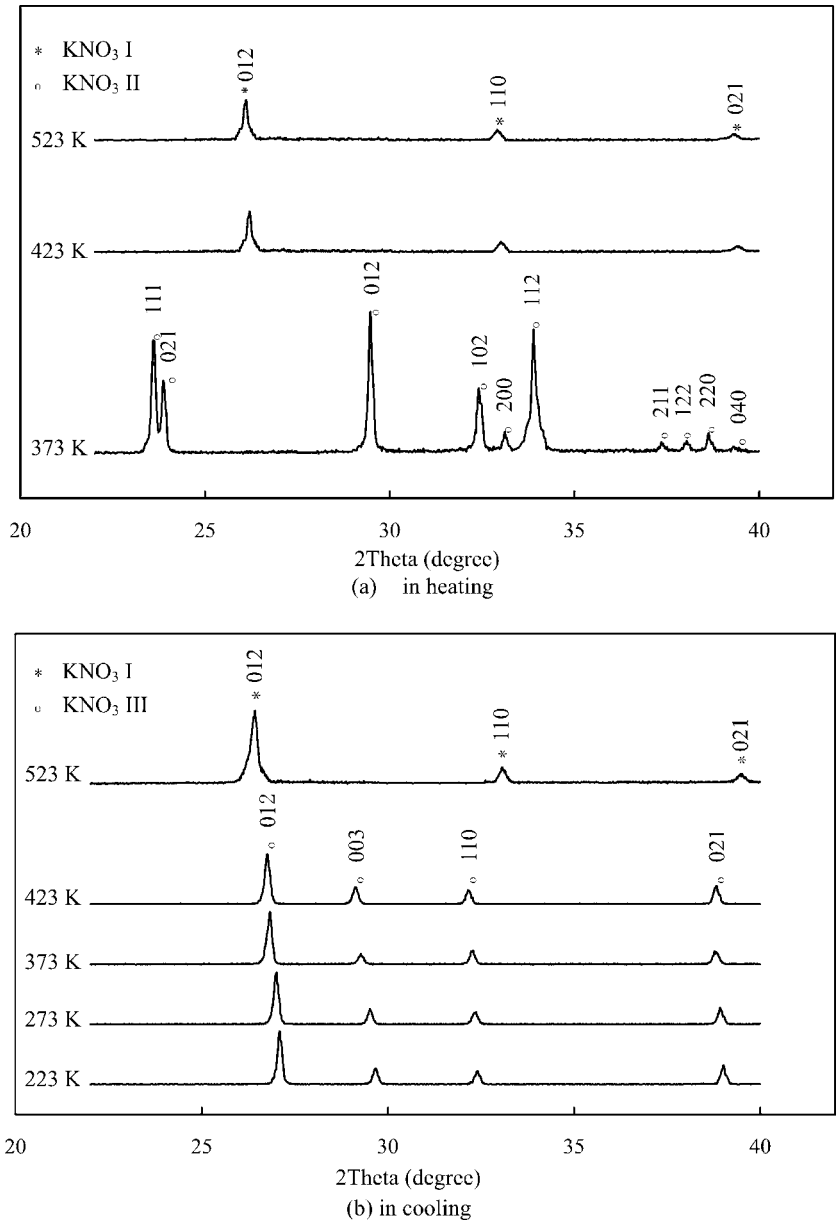

Fig. 3. High-temperature X-ray diffraction pattern for $x_{KClO_3} = 0.05$.

$KClO_3$ crystals belong to monoclinic ($P2_1/m$), and K-ions and ClO_3-radicals make a NaCl-type configuration in this crystal [10]. For the sake of trigonal pyramidal structure of the ClO_3-radical, the K-ions and the ClO_3-radicals make a monoclinic lattice. For the structure of KNO_3 crystal in phases I and III, the K-ions and the NO_3-radicals make a similar configuration to the NaCl-type, while the structure of regular triangular plane of the NO_3-radical makes KNO_3 crystal be trigonal. For the resemblance of structures of both substances the solid solution KNO_3–$KClO_3$ is expected to be formed to some extent. Limited solid solutions in KNO_3-rich regions was noted by some researchers recently, too [6,7].

We could get transparent solid solutions of $K(NO_3)_{1-x}(ClO_3)_x$ from the quenched samples ($x = 0.05$ and 0.20), and the transition temperature $T_{III–II}$ of the solid solution was lowered to room temperature, X-ray diffraction patterns of both phases I and III were observed at about examined temperature.

The temperatures and enthalpies of fusion of KNO_3 and $KClO_3$ were used in Eqs. (1)–(3) to obtain the thermodynamic excess properties and other parameters. The liquidus and the solidus can be calculated from the simultaneous equations for components A and B. Simultaneous least-squares optimization of Solver in Microsoft Excel® were used in the calculation [11]. As a verification of the validity of the least-squares optimization method of Solver, it was applied to calculate the phase diagram of CsCl(A)–CsI(B), which forms limited solid solutions with

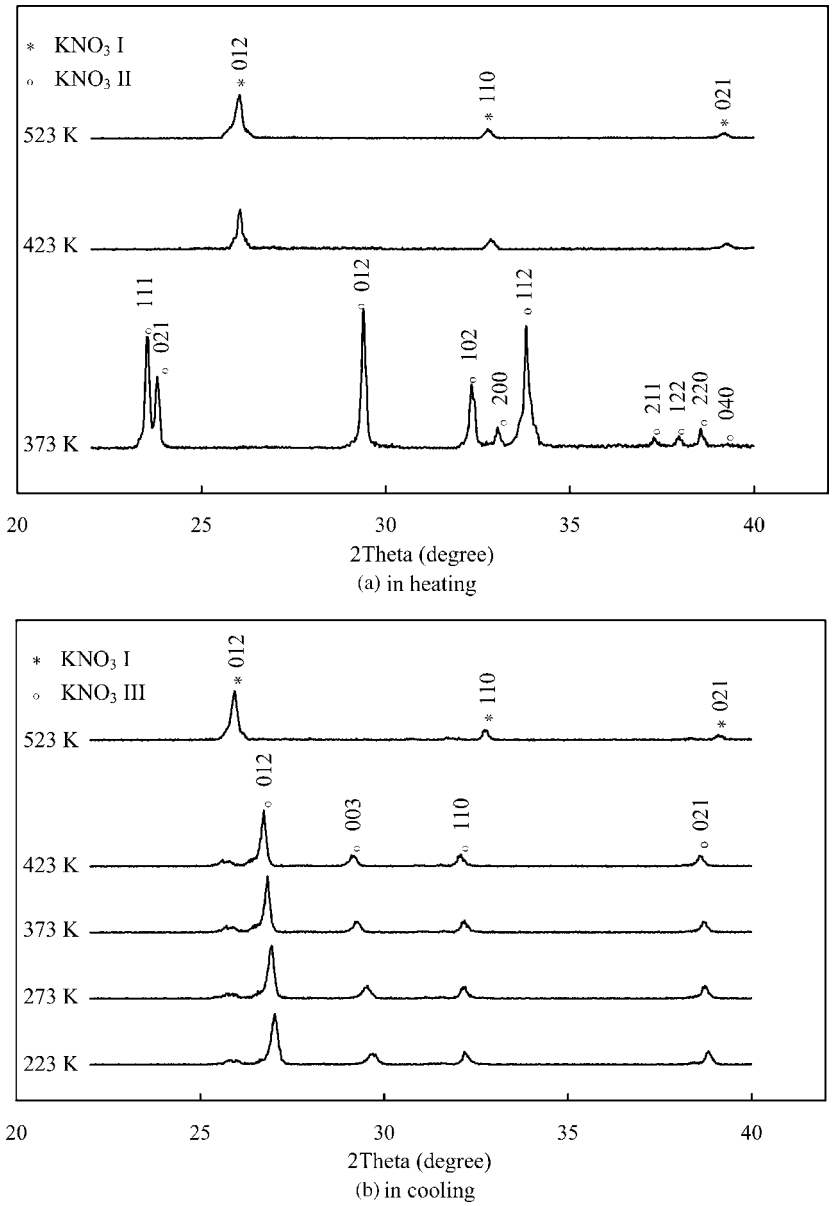

Fig. 4. High-temperature X-ray diffraction pattern for $x_{KClO_3} = 0.20$.

an eutectic point homologous to KNO_3–$KClO_3$. The results agreed well with those calculated by Sangster using the F*A*C*T system [12].

The excess enthalpy of the liquid is given as follows:

$$H^{E}(l)\ (\mathrm{J\,mol^{-1}}) = x_A x_B(-1406.5 - 312.1x_A) \quad (4)$$

For the α-solid phase, a Henrian activity coefficient for $KClO_3$ in KNO_3 at the eutectic temperature is given by

$$G_B^{E}(s,\alpha)\ (\mathrm{J\,mol^{-1}}) = H^{E}(s,\alpha) = RT\ln\gamma_B = 5400 \quad (5)$$

For the β phase, the expression is

$$H^{E}(s,\beta)\ (\mathrm{J\,mol^{-1}}) = 7648x_A x_B \quad (6)$$

Both the quantities were assumed to be independent of temperature.

The calculated eutectic is 556 K at $x_B = 0.31$ and the limits of solid solubility at the eutectic temperature are $x_B = 0.20$ and 0.90, respectively. Probable maximum inaccuracy in calculated liquidus is ±10 K (Figs. 1 and 4). The limit of solid solubility for KNO_3-based solid solution was the same as obtained by Velikhov et al. [7]. The phase diagram clearly indicates that the system KNO_3–$KClO_3$ is a limited solid solution system. However, the phase diagram was described as a simple eutectic system previously. The calculated phase diagram is overlaid on the examined phase diagrams over a wide range of composition and temperature within the experimental error limits in Fig. 1. For KNO_3-based solid solution, during cooling the KNO_3 ferroelectric phase can be stabilized down below 223 K (Fig. 5).

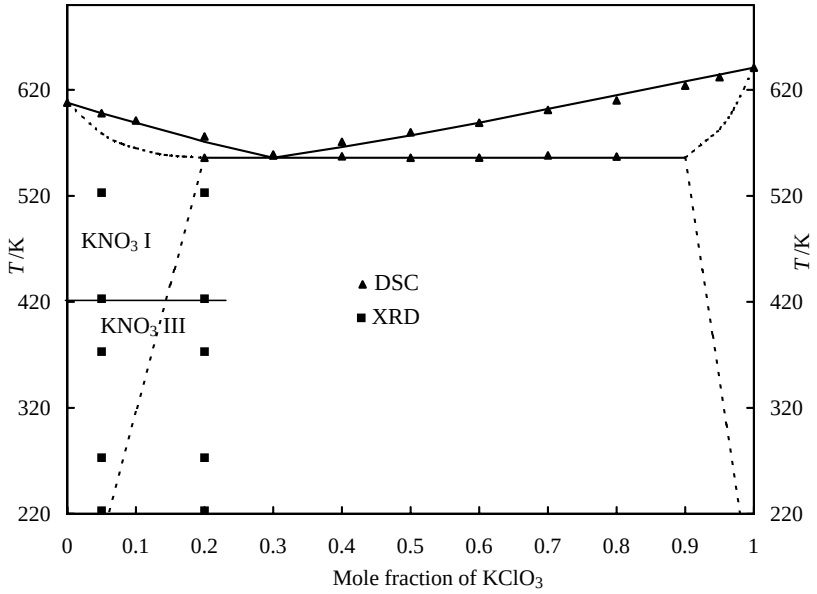

Fig. 5. The phase diagram for the KNO_3–$KClO_3$ system during cooling.

5. Conclusions

The limited solid solutions, $K(NO_3)_{1-x}(ClO_3)_x$ ($0 < x < 0.20$) and $K(NO_3)_{1-x}(ClO_3)_x$ ($0.90 < x < 1.0$) were formed in the KNO_3-based solid solutions and $KClO_3$-based solid solutions phase. During cooling the KNO_3 ferroelectric phase can be stabilized from 423 K down below 223 K by the KNO_3-based solid solution $K(NO_3)_{1-x}(ClO_3)_x$ ($0 < x < 0.20$) as a result of substitution of NO_3 by ClO_3-radicals. The solidus and liquidus, calculated using least-squares optimization based on limited solid solutions, which represent closer to the experimental data, are obtained. The eutectic is 556 K at $x_B = 0.31$ and the solid solubilities of KNO_3-based (α) phase and $KClO_3$-based (β) solid solutions are $x_B = 0.20$ and 0.90 at the eutectic temperature, respectively. The formation of the solid solutions in the KNO_3–$KClO_3$ system can be easily understood because of the similar structure and the small difference in the ionic radii of the anions. This result is identical with thermodynamic calculation.

References

[1] R. Murugan, A. Ghule, H. Chang, J. Appl. Phys. 86 (1999) 6779.
[2] B.V. Schonwandt, H.J. Jakobsen, J. Solid State Chem. 145 (1999) 10.
[3] S. Shimada, T. Aoki, Thermochim. Acta 283 (1996) 323.
[4] M. Midorikawa, Y. Takagi, Y. Ishibashi, J. Phys. Soc. Jpn. 28 (1970) 1001.
[5] A.Ya. Dantsiger, Sov. Phys. Solid State 7 (1966) 1845.
[6] Y. Takeuchi, Ferroelectrics 165 (1995) 263.
[7] Yu.N. Velikhov, V.M. Ishchuk, V.D. Panikarskaya, T.S. Teplitskaya, Inorg. Matter (Trans. Neorg. Mater.) 32 (1996) 1845.
[8] N.K. Voskresenskaya (Ed.), Handbook of Solid–Liquid Equilibria in Systems of Anhydrous Inorganic Salts, vol. I, Kete Press, Jerusalem, 1970.
[9] Y. Dessureault, J. Sangster, A.D. Pelton, J. Chim. Phys. 87 (1990) 407.
[10] G.N. Ramachandran, M.A. Lonappan, Acta Crystallogr. 10 (1957) 281.
[11] X.J. Zhang, K.C. Xu, Y.C. Gao, Thermochim. Acta 385 (2002) 81.
[12] J. Sangster, A.D. Pelton, J. Phys. Chem. Ref. Data 16 (1987) 509.